Transient Absorption and Time-Resolved Raman Study of the Photophysics of 4-Phenylpyridine in Solution

G. Buntinx,* R. Naskrecki,† and C. Didierjean

Laboratoire de Spectrochimie Infrarouge et Raman (LASIR) du CNRS, Centre d'Etudes et de Recherches Lasers et Applications, Université de Lille I, 59655 Villeneuve d'Ascq, France

O. Poizat*

Laboratoire de Spectrochimie Infrarouge et Raman (LASIR), CNRS, 2 rue Henri-Dunant, 94320 Thiais, France

Received: July 10, 1997; In Final Form: September 12, 1997[⊗]

The transient absorption spectra and time-resolved resonance Raman spectra of 4-phenylpyridine (4PPY) in various organic solvents have been measured following pulsed photolysis at 266 nm using nanosecond and picosecond time resolution experiments. The T_1 and S_1 states are characterized and attributed to $\pi\pi^*$ and $n\pi^*$ configurations, respectively, in aprotic solvents as well as in alcohols and water. In the presence of alcohols, both the S_1 and T_1 states are reduced to the same transient product, the *N*-hydro radical 4PPYH•. The overall photophysical properties of 4PPY appear similar to those previously found for the diaza analogue, 4,4′-bipyridine. Vibrational analyses of the S_1 and T_1 states and of the radical 4PPYH• are proposed and compared with results reported in the literature for the neighboring compounds biphenyl and 4,4′-bipyridine. The structure and electronic configuration of these transients are discussed on this basis.

1. Introduction

The photophysical properties of aza-aromatic compounds are mainly governed by the existence of close-lying, vibronically interacting $n\pi^*$ and $\pi\pi^*$ levels in the region of the lowest singlet (S_1) and triplet (T_1) excited states.[1,2] The energy gap and relative positions of these levels varying with the solvent polarity and protic character, the strengths of the vibronic and spin−orbit couplings, and thus the quantum yields of luminescence and of radiationless processes are generally also strongly solvent dependent.

The photophysics of 4-phenylpyridine (4PPY) in solution has been studied by luminescence[3−5] and time-resolved EPR.[3,6] The long decay times found at 77 K for the phosphorescence signal in methanol−water solution (3 s)[3] or in ethanol−isopentane−ethyl ether (EPA) solution (2.1 s),[4] and for the EPR signal in ethanol (2.6 s),[6] are in agreement with the $^3A_1(\pi\pi^*)$ nature predicted for the T_1 state of 4PPY from CNDO/S calculations.[4] On the other hand, 4PPY has been found nonfluorescent in organic solvents such as cyclohexane, acetonitrile, and methanol, but fluorescent in water and in acidic aqueous solution.[4] CNDO/S calculations[4] predict that the S_1 state is $^1B_2(n\pi^*)$ in 4PPY but interchanges with a nearby $^1A_1(\pi\pi^*)$ state in the protonated molecule $4PPYH^+$ as the $n\pi^*$ level is raised to higher energy. On this basis and according to El-Sayed's selection rules[7,8] for intersystem crossing, the absence of fluorescence for 4PPY is explained[4,5] as due to a very fast intersystem crossing (ISC) between $^1n\pi^*$ and $^3\pi\pi^*$ states, whereas the appearance of fluorescence on protonation is the consequence of a much slower ISC between $^1\pi\pi^*$ and $^3\pi\pi^*$ states for which first-order spin−orbit coupling is forbidden. The fluorescence quantum yield in water is found comparable to that in acidic solution although the molecule is not protonated in the ground state. The authors conclude that 4PPY protonates in the excited state. More recently, the fluorescence properties of 4PPY were alternately considered[9] as governed by the strength of vibronic interactions between the $^1n\pi^*$ and $^1\pi\pi^*$ states, according to a mechanism proposed by Lim:[2,10] in inert solvents both states are close together and strongly coupled in such a way that fast internal conversion ($S_1 \rightarrow S_0$) quenches the fluorescence; in acidic solutions the increase in energy of the $^1n\pi^*$ state due to the interaction with the solvent hinders the vibronic interactions, and the fluorescence is thus enhanced.

In the present work we present the first investigation of the 4PPY photophysics by transient absorption and time-resolved resonance Raman. Two types of pump/probe experiments differing by their time resolution were used: laser flash photolysis and Raman scattering in the nanosecond to millisecond time domain on one hand and subpicosecond absorption and picosecond Raman scattering on the other. These results are compared with those reported for the neighboring aromatic molecules biphenyl,[11−20] 4,4′-bipyridine,[21−27] and 2,2′-bipyridine.[26,29] Part of the nanosecond Raman results have been already shortly mentioned in a previous review paper.[30]

2. Experimental Section

4-Phenylpyridine (Aldrich) was carefully dried in vacuo to remove hydration water and sublimated at 80 °C in vacuo prior to each measurement. 2,2,2-Trifluoroethanol (Lancaster) and nonfluorinated solvents (Prolabo) were used as received. Water was doubly distilled and deionized (Milli-Q plus ultrapure water system from Millipore). Transient spectroscopic experiments in the nano/microsecond time domain were performed on deaerated, Ar-purged sample solutions at concentrations varying from 10^{-4} to 10^{-5} M (absorption measurements) and from 5×10^{-3} to 10^{-3} M (Raman measurements). Subpicosecond absorption and picosecond Raman measurements were carried out on 5×10^{-3} to 10^{-4} M solutions. These solutions were not deaerated.

The transient absorption experiment in the microsecond time domain has already been described.[31] The pump beam at 248 nm (1.5 mJ, 20 ns) is provided by an excimer laser (Questeck

* Corresponding author.
†Permanent address: Department of Physics, Poznan University, Grunwaldzka 6, 60780 Poznan, Poland.
⊗ Abstract published in *Advance ACS Abstracts,* November 1, 1997.

S1089-5639(97)02250-0 CCC: $14.00

2040) and focused on a 1 × 10 mm^2 slice of the sample, yielding a 15 mJ/cm^2 energy density per pulse. The probe light (1 mm diameter) is provided by a pulsed xenon lamp (Applied Photophysics). The detector, a photomultiplier (Hamamatsu 1P28) coupled to a digital oscilloscope (Tektronix TDS540), allows a 0.1 μs time resolution.

The nanosecond Raman experiment (description in refs 17 and 32) uses the excimer laser for the pump pulse (248 nm, 1 mJ, about 1.5 J/cm^2, 20 ns), a Nd:YAG + dye laser system (Quantel 581C and TDL50) for the probe pulse (355, 370, and 532 nm, 7−10 ns, 1 mJ), a gated intensified diode array (20 ns gate) as detector, and a home-built spectrometer. The spectral resolution and the analyzed field are about 9 and 1750 cm^{-1} at 355 nm, 8 and 1600 cm^{-1} at 370 nm, and 5.5 and 1100 cm^{-1} at 532 nm. The probe pulse is delayed relative to the pump using a homemade pulse and delay generator.

Subpicosecond and picosecond experiments were carried out by using a Ti−sapphire laser system based upon a Coherent (MIRA 900D) oscillator and a BM Industries (ALPHA 1000) regenerative amplifier. The oscillator can be utilized in two different configurations providing either 90 fs or ≅2 ps pulses (1 W), leading after amplification to 100 fs (1 mJ) or ≅2.5 ps (0.8 mJ) pulses, respectively, at 800 nm (1 kHz) and, after frequency tripling (0.5 or 2.0 mm BBO crystals, respectively), to 100 μJ pulses at 266 nm. The UV−visible absorption experiment, performed in the subpicosecond laser configuration, has been described in detail previously.[26] It uses the tripled laser output at 266 nm (35−40 μJ, 4.5−5 mJ/cm^2 per pulse) as pump pulse, a continuum probe pulse generated at 800 nm, and an intensified double photodiode array (DILOR) as detector. The pump−probe polarization configuration is set at the magic angle. The continuum probe pulse is delayed in time relative to the pump pulse using an optical delay line (Microcontrol Model MT160-250PP driven by an ITL09 controller, precision ±1 μm). The overall time resolution (fwhm of the pump/probe intensity cross-correlation) at a given wavelength is estimated to be about 400 fs from the two-photon absorption risetime in pure hexane. The time dispersion of the continuum light over the 300−670 nm region is about 0.8 ps. The spectra shown in this report are not corrected for this dispersion effect. The time origin is arbitrarily chosen as the maximum overlap of the pump and probe pulses at 400 nm: signals in the 540−580 nm region are delayed (real time ≈ t − 400 fs), and those in the 320−340 nm region are in advance (real time ≈ t + 200 fs) with respect to this reference time. Data were accumulated over 3 min (≈180 000 pump−probe sequences).

Raman measurements were achieved in the picosecond laser configuration, the pump and probe beams being the third (247−266 nm, 20 μJ, 25 mJ/cm^2 per pulse) and second (370−400 nm, 10−20 μJ) harmonics, respectively, of the Ti−sapphire fundamental (740−800 nm). The pump/probe cross-correlation fwhm is 5 ps. The probe beam traverses the optical delay line before being focused with a 30 cm lens collinearly to the pump beam on the sample contained in a flow cell. The zero time position of the experience was determined using the difference frequency generation technique between the pump and probe pulses in a BBO crystal. All spectra are measured at the magic angle. Scattered light is collected at 90° to the incident excitation, passes through a Notch filter, and is dispersed in a home-built multichannel spectrometer coupled to a CCD optical multichannel analyzer (Princeton Instrument LN-CCD-1100-PB-UV/AR detector + ST-138 controller). The wavenumber shift is calibrated using the Raman spectra of indene. Data collection times were 5−30 min.

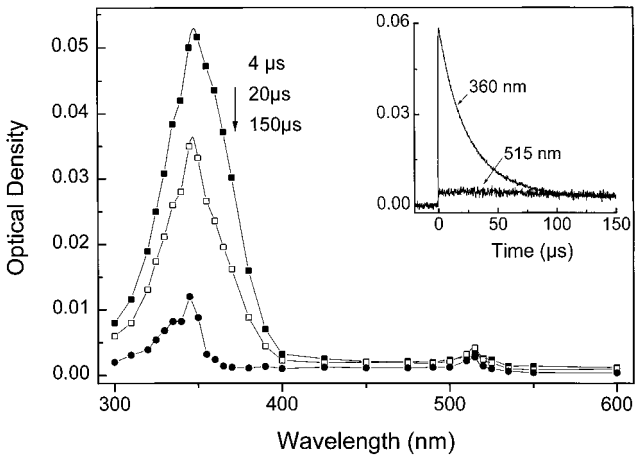

Figure 1. Transient absorption spectra of a deaerated solution of 4PPY (10^{-4} M) in *n*-hexane at different times following nanosecond laser photolysis at 248 nm. The insert shows the kinetic traces taken at 360 and 515 nm.

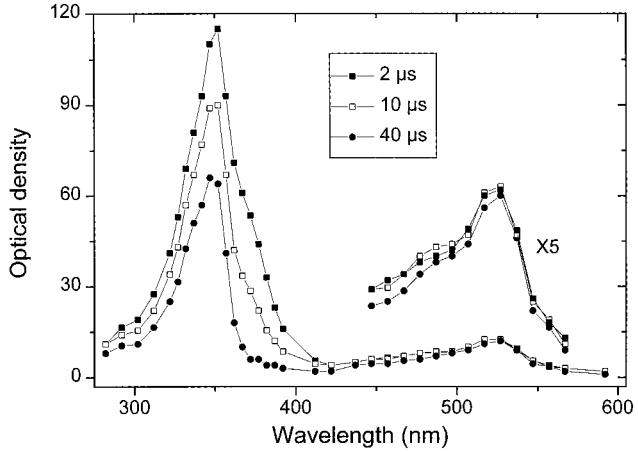

Figure 2. Transient absorption spectra of a deaerated solution of 4PPY (10^{-4} M) in methanol at different times following nanosecond laser photolysis at 248 nm.

3. Results and Discussion

3.1. Photophysics of 4PPY in the Nanosecond−Microsecond Time Range. The photophysical behavior of 4PPY in acetonitrile, cyclohexane, *n*-hexane, water, methanol, ethanol, and 2-propanol was investigated by transient absorption in the nano- to millisecond time domain after nanosecond pump excitation at two wavelengths, 266 and 248 nm. These excitation lines fall within a strong absorption band of 4PPY peaking at 255 nm ($\epsilon_{max} \sim 16\,000$ M^{-1} s^{-1}), which corresponds to the optically allowed $S_0 \rightarrow S_n$ ($\pi\pi^*$) transition of lowest energy. Comparable results were obtained with both excitations. Time-resolved Raman measurements were also performed following photolysis at 248 nm. Figures 1 and 2 show the transient absorption spectra recorded at different times after 248 nm excitation of deaerated solutions of 4PPY (10^{-4} M) in *n*-hexane and in methanol, respectively. In *n*-hexane and cyclohexane the spectra present essentially one band at 352 nm which decays with mixed first-order and second-order kinetics. This absorption appears strongly quenched in the presence of oxygen. Similar spectra are observed in water ($\lambda_{max} = 357$ nm) and acetonitrile ($\lambda_{max} = 352$ nm), but their intensity is 3−4 times higher than in alkanes. They are unambiguously ascribed to the lowest triplet state T_1 in regard to their long lifetime and their sensitivity to oxygen. Accordingly, the time-resolved Raman spectra recorded in these solvents in resonance with this absorption are assigned to the T_1 state. As an example, part A

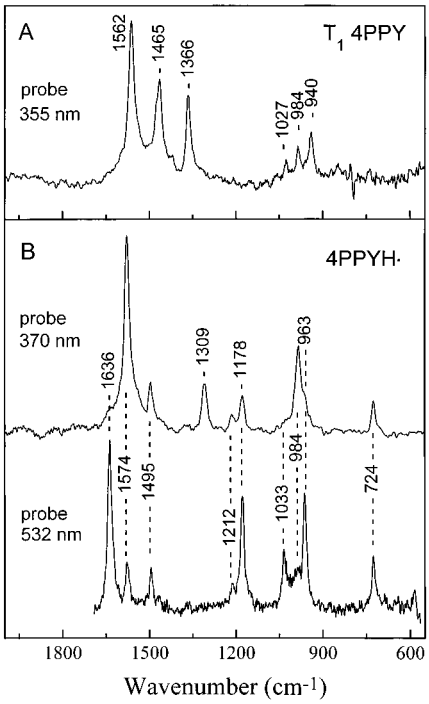

Figure 3. Time-resolved resonance Raman spectra of (A) the triplet-state T_1 4PPY probed at 355 nm, 30 ns after 248 nm excitation of a deaerated solution of 4PPY (5×10^{-3} M) in cyclohexane, and (B) the *N*-hydro radical 4PPYH• probed at 370 nm (upper trace) and 532 nm (lower trace) 500 ns after 248 nm excitation of a deaerated solution of 4PPY (5×10^{-3} M) in methanol. Solvent bands are subtracted in all cases.

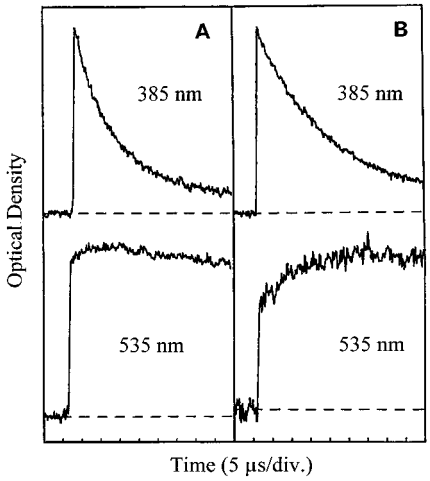

Figure 4. Transient absorption kinetics at 385 nm (upper trace) and 535 nm (lower trace) following nanosecond laser excitation at 248 nm of 10^{-4} M solutions of 4PPY in (A) methanol and (B) 2-propanol.

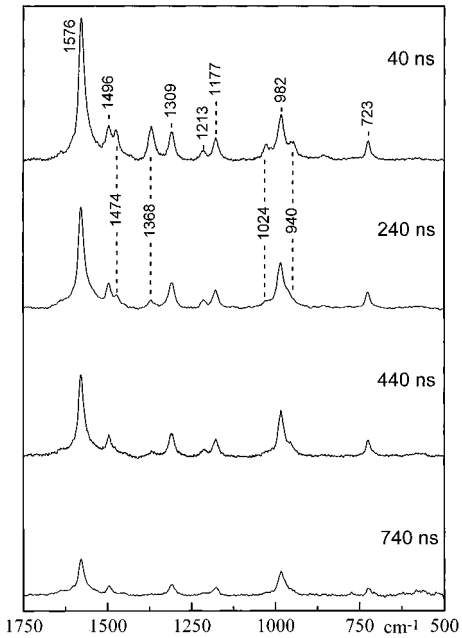

Figure 5. Time-resolved resonance Raman spectra (probe 370 nm) of a deaerated solution of 4PPY (5×10^{-3} M) in methanol at different times following nanosecond laser photolysis at 248 nm. All spectra are normalized with respect to the solvent bands which have then been subtracted. The band wavenumbers given in the 40 ns spectrum characterize the 4PPYH• radical. The dashed lines designate the main bands of the T_1 state.

in Figure 3 shows the triplet-state Raman spectrum of 4PPY in cyclohexane probed at 355 nm. The spectrum recorded in acetonitrile is comparable, but, due to the high solvent polarity, the triplet lines are shifted by a few wavenumbers and additional weak lines are observed at 1606, 1486, 1320, 1225, 985, and 737 cm^{-1}, which are probably due to the cation radical $4PPY^{\bullet+}$ produced by ionization. The photoionization of biphenyl in acetonitrile has been observed in similar experimental conditions.[15,17,18] As a confirmation, these additional lines are not present in basicified solutions such as acetonitrile/KOH or acetonitrile/ triethylamine. On the other hand, a very weak residual absorption spectrum with bands at 345 and 515 nm is observed after complete decay of the T_1 absorption in *n*-hexane and cyclohexane (150 μs spectrum in Figure 1) but not in water and acetonitrile. The kinetic trace at 515 nm decays in about 1 ms and is nearly constant on a 0−20 μs time range, indicating that the long-lived species does not proceed from the T_1 state but is formed at very short time.

In the presence of reductors such as triethylamine, 4,4′-bipyridine was found to be efficiently photoreduced in acetonitrile via quenching of the T_1 state by electron transfer.[23] In contrast, no photoreduction by triethylamine is observed in the case of 4PPY, probably due to a higher oxidation potential ($E_{1/2}$ vs $Ag/Ag^+ = -2.24$ V) compared to that of 4,4′-bipyridine ($E_{1/2} = -1.91$ V).[33]

The 2 μs absorption spectrum recorded for a methanol solution of 4PPY (Figure 2) shows clearly two bands at 355 and 525−530 nm. At a delay of 40 μs the visible band remains nearly unchanged, but the UV line is less intense and notably narrower. After 40 μs there is no more change in band shape, and a common, slow decay kinetics is observed at all wavelengths. The 40 μs spectrum in Figure 2 characterizes thus a single transient species. Subtracting this spectrum from the 2 μs trace after normalization relative to the 525 nm band yields a spectrum very similar to that shown in Figure 1 for the T_1 state. Therefore, the 2 μs spectrum results from the superposition of absorptions due to the triplet-state and the long-lived species. Comparable results are obtained in ethanol and 2-propanol solutions. The time evolution of the two transient species, monitored respectively at 385 nm, where mainly T_1 absorbs, and at 535 nm, where there is no contribution from T_1, are displayed in Figure 4 for methanol (part A) and 2-propanol (part B) solutions. Figure 5 shows transient resonance Raman spectra recorded at 370 nm, which is in close resonance with the UV absorption bands of both the triplet-state and the long-lived species, at different times after 248 nm excitation of a 5×10^{-3} M solution of 4PPY in methanol. A first group of Raman lines at 1474, 1368, 1024, and 940 cm^{-1}, which disappears within 700 ns, corresponds to the triplet-state features. A second series of lines at 1576, 1496, 1309, 1213, 1177, 982, and 723 cm^{-1}, not observed in acetonitrile, water,

and alkanes, are likely corresponding to the species responsible for the long-lived transient absorption. Subtracting the 740 ns spectrum from the 40 ns one after normalization with respect to the 1309, 1177, and 723 cm^{-1} peak intensities leads to a spectrum very similar to that shown in part A of Figure 3, which confirms the assignment of the former, short-lived group of Raman lines to the triplet state. Note that the decay times found from these Raman data are much shorter than those deduced from the absorption measurements. This effect has been commonly encountered in previous combined investigations of reaction kinetics by transient absorption and transient Raman spectroscopies.[23,25,28] It results from the fact that, because of the low sensitivity of the Raman technique compared to absorption, much higher sample concentration and pump energy conditions are needed, leading to much higher concentrations in photoproducts and thus promoting multimolecular decay processes.

The appearance of the long-lived species (535 nm traces in Figure 4) shows a double, fast (unresolved) and slow, kinetics. The slow component is almost negligible in methanol and ethanol but becomes more significant in 2-propanol. It can be fit by the same kinetics as the decay of the triplet state. To identify this species, it is worthwhile to consider the photoreactivity of 4,4′-bipyridine (44BPY). We recently found[25,26] that the photoexcitation of 44BPY in alcohols results in the formation of the *N*-hydro radical $NC_5H_4-C_5H_4NH^{\bullet}$ (44BPYH$^{\bullet}$) from two different processes: a slow reaction of abstraction by the T_1 state of a hydrogen atom from the alcohol solvent ($k_q \sim 10^5$ M^{-1} s^{-1}) and an ultrafast, nondiffusional process involving the very short-lived excited singlet state S_1 ($k \sim 10^{10}$ s^{-1}) via a mechanism that is not yet clearly understood. The difference in reactivity of the T_1 and S_1 states was attributed to their different nature ($\pi\pi^*$ and $n\pi^*$, respectively). By analogy, we ascribe the long-lived species formed upon excitation of 4PPY in alcohols to the *N*-hydro radical $C_6H_5-C_5H_4NH^{\bullet}$ (noted hereafter as 4PPYH$^{\bullet}$). In fact, its double kinetics appearance, the fact that T_1 is the precursor state in the slow process and that the contribution of this slow process is proportional to the H atom donor character of the alcoholic solvent, can be compared to the appearance characteristics of 44BPYH$^{\bullet}$. In addition, the long-lived transient absorption spectrum in Figure 2 (40 μs spectrum) resembles closely that found for the 44BPYH$^{\bullet}$ radical (band maxima at 370 and 540 nm).[23,25] The transient Raman spectra of 4PPYH$^{\bullet}$ probed in resonance with its two absorption bands ($\lambda_{probe} = 370$ and 532 nm) are displayed in part B of Figure 3. They show very specific resonance enhancement effects. As discussed further in section 3.5, these effects and the peak wavenumbers are comparable to those characterizing the 44BPYH$^{\bullet}$ radical.[22] These spectroscopic analogies confirm that the 4PPYH$^{\bullet}$ radical is the photoproduct formed in alcohols besides the T_1 state. Rate constants for quenching of T_1 by methanol and 2-propanol of about 0.6×10^5 and 0.9×10^5 M^{-1} s^{-1} were obtained from pseudo-first-order analyses in alcohol/acetonitrile mixtures. Note finally that the weak residual spectrum observed in *n*-hexane and cyclohexane after complete decay of the T_1 state (150 μs spectrum in Figure 1) can be also ascribed to the *N*-hydro radical as it is comparable to the radical spectrum in alcohols (40 μs spectrum in Figure 2). To characterize the S_1 state of 4PPY and to get a better insight into the photophysics and photochemical reactivity of this molecule in solution, we have performed time-resolved spectroscopic measurements in the picosecond time domain.

3.2. Photophysics of 4PPY in the Picosecond Time Range. Transient absorption measurements on solutions of 4PPY in acetonitrile, *n*-hexane, cyclohexane, water, methanol, ethanol, 2-propanol, 2,2,2-trifluoroethanol (TFE), and water/HCl at pH 1 were performed at different times in the 0−500 ps range following subpicosecond excitation at 266 nm. Figures 6−9 show a selection of typical spectra obtained for solutions of 4PPY (10^{-3} M) in acetonitrile, *n*-hexane, water, and methanol, respectively. In the case of methanol measurements at different concentrations between 10^{-4} and 5×10^{-3} M were realized. No perceptible influence of the concentration on the spectral evolution was observed in this range.

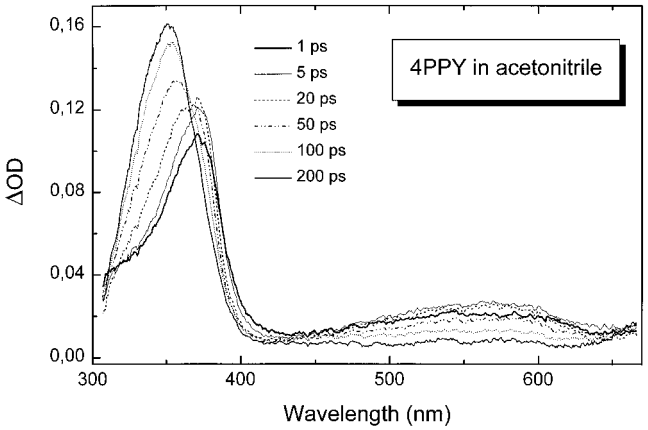

Figure 6. Transient absorption spectra of 10^{-3} M 4PPY in acetonitrile measured at different delay times following femtosecond laser photolysis at 266 nm.

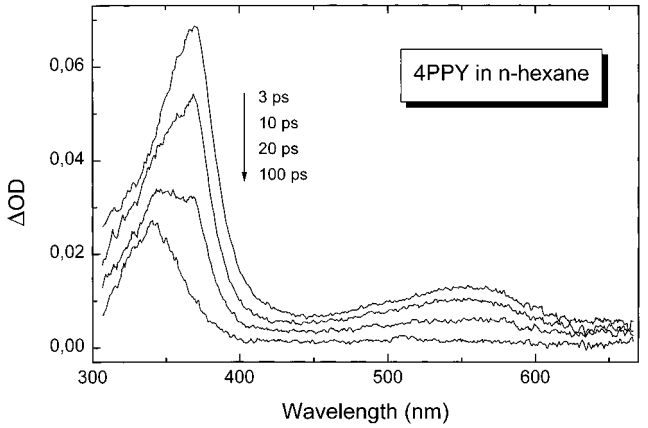

Figure 7. Transient absorption spectra of 10^{-3} M 4PPY in *n*-hexane measured at different delay times following femtosecond laser photolysis at 266 nm.

The 200 ps spectrum in acetonitrile (Figure 6) presents a single band at 352 nm which corresponds to the spectrum characterized above in the microsecond time scale for the triplet state T_1 (4 μs spectrum in Figure 1 for example). The 1 ps spectrum displays two bands at 370 and 575 nm which grow and narrow slightly from 1 to 20 ps then decay whereas the T_1 band appears. The decay at 575 nm and the growth of the triplet absorption can be correctly fit by the same monoexponential kinetics ($\tau_{1/2} = 100$ ps), and an isosbestic point is observed at 365 nm for delay times longer than 20 ps. We ascribe thus the short-time spectrum to the first excited singlet state S_1 of 4PPY. The lack of an isosbestic point at shorter times is due to the increase of the S_1 band itself in the 0−20 ps time delay as noted above. In *n*-hexane (Figure 7), the 3 ps spectrum is comparable to that found for the S_1 state in acetonitrile and leads essentially to the T_1 absorption after complete decay (100 ps spectrum). However, the S_1 lifetime is much shorter ($\tau_{1/2} = 22$ ps), and the bands are slightly blue-shifted ($\lambda_{max} = 368$ and 555 nm). Moreover, in agreement with the results obtained in the nano/

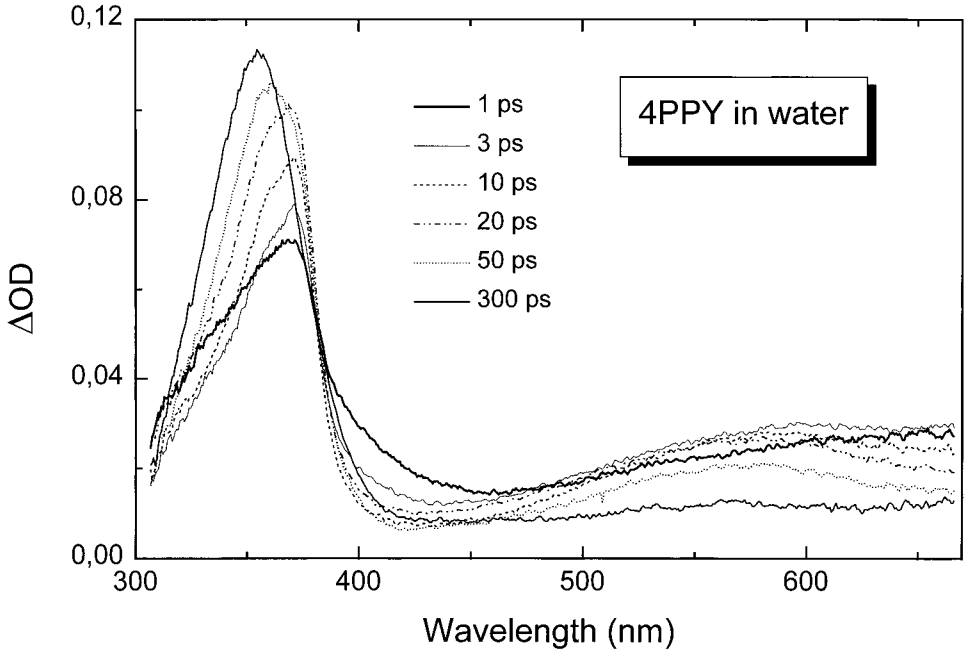

Figure 8. Transient absorption spectra of 10^{-3} M 4PPY in water measured at different delay times following femtosecond laser photolysis at 266 nm.

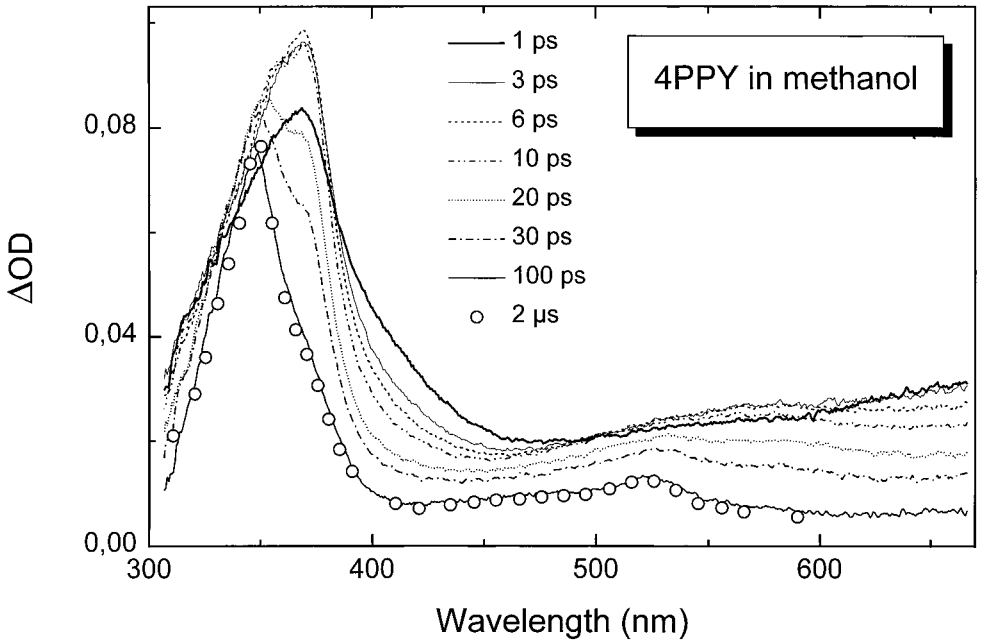

Figure 9. Transient absorption spectra of 10^{-3} M 4PPY in methanol measured at different delay times following femtosecond laser photolysis at 266 nm. The 2 μs spectrum obtained with the nanosecond excitation experiment (same as in Figure 2) is also plotted for comparison.

microsecond experiment, the intensity of the T_1 absorption relative to the S_1 spectrum appears notably weaker in *n*-hexane than in acetonitrile. Similar data are obtained in cyclohexane.

Consider now the spectral evolution observed in water (Figure 8). At 1 ps the spectrum appears notably different from those found in acetonitrile or *n*-hexane. Its UV band, also peaking at 370 nm, is prolonged by a broad wing extending on its red side from 390 to 450 nm. In the visible region a very broad band beginning at 450 nm and maximizing beyond 670 nm is observed. This spectrum evolves rapidly from 1 to 20 ps, decreasing in intensity in the 400−450 and 600−670 nm regions and intensifying at 370 nm and in the 500−600 nm range. This change leads to a spectrum (20 ps spectrum in Figure 8) with band maxima at 370 and 575 nm comparable to the S_1 spectrum observed in acetonitrile and *n*-hexane. Then the S_1 spectrum decays to yield the T_1 features. The short-time dynamics will be discussed later (see section 3.5). It is worthy to mention that no perceptible gain signal is detected. In contrast, no satisfying measurement of the $S_1 \rightarrow S_n$ absorption spectrum could be made in TFE and in H_2O/HCl (pH 1) acidic solutions due to a strong gain signal below 450 nm.

The spectra recorded in methanol (Figure 9), ethanol, and 2-propanol show the same evolution as in water at short times: an initial spectrum with a broad absorption in the 300−450 nm region peaking at 370 nm and a second broad signal maximizing beyond 670 nm relaxes in 10−20 ps to yield the typical S_1 spectrum. At longer delay times this S_1 spectrum decays within 50 ps and leads to new absorptions at 350 and 525 nm, which correspond to the superposition of the T_1 state and the *N*-hydro radical features, as observed above (Figure 2) in the 2 μs spectrum obtained by using the nanosecond excitation configuration. This spectrum is also plotted in Figure 9 for compari-

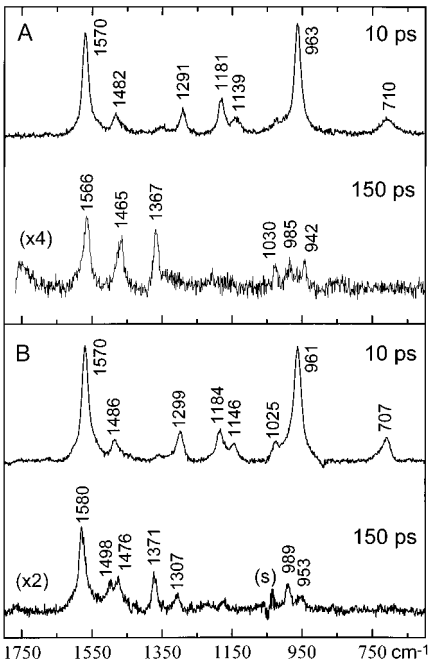

Figure 10. Time-resolved resonance Raman spectra of solutions of 4PPY (5×10^{-3} M) in (A) *n*-hexane and (B) methanol, probed at 380 nm at delay times of 10 ps (upper trace) and 150 ps (lower trace) following picosecond laser excitation at 253 nm. All spectra are normalized with respect to the solvent bands which have then been subtracted. The symbol (s) indicates an artifact of subtraction of the intense methanol line at 1035 cm^{-1}.

son. The evident analogy of the two traces confirms that there is a correlation between the results obtained in the two configurations of excitation; i.e., the same overall reactivity is observed in the two experiments despite quite different excitation conditions. (The instantaneous photon density of the femtosecond pump is about 25 000 times that of the nanosecond pump.) In particular, the relative amounts of triplet-state and radical species produced in the two cases are equal. We conclude that there is no significant perturbation due to multiphoton absorption processes in the subpicosecond measurements. The above results show the formation of the T_1 state from S_1 and of the 4PPYH$^\bullet$ radical within 50 ps in alcohols. Then these two species appear approximately stable on a 50 ps-1 μs time range and react on a microsecond time scale. However, as seen in Figure 9, the S_1 absorption is overlapping the radical spectrum at all wavelengths in such a way that it is not possible to determine from these absorption data whether the radical arises from the S_1 state or it is formed directly in parallel to the S_1 state. We have thus undertaken time-resolved measurements in the picosecond time scale by resonance Raman spectroscopy which allows usually a more specific characterization of species having close electronic spectra.

We have obtained transient resonance Raman spectra of 4PPY in *n*-hexane, methanol, ethanol, acetonitrile, and water, over the range from 300 to 1800 cm^{-1}, at various delays from 2 to 150 ps using a probe excitation at 380 nm and a pump excitation at 253 nm. Figure 10 shows the 8 and 150 ps spectra recorded in *n*-hexane and methanol. For methanol solutions, a few spectra excited at 400 nm (pump excitation at 266 nm) in the 2$-$20 ps time range appeared similar to those excited at 380 nm. Measurements were also performed in the anti-Stokes region (-300 to -1800 cm^{-1}). We could not detect any signal in this region even at zero time delay (pump and probe superposed). Apart from slight differences in band wavenumbers ($\Delta\nu \leqslant 7$ cm^{-1}) and relative intensities, the Stokes spectra found at short time (e.g., 10 ps spectra in Figure 10) are similar in all solvents. They are ascribed to the S_1 state as they present nearly the same decay times as the related $S_1 \rightarrow S_n$ transient absorption spectra. As a confirmation, the decay of the S_1-state Raman spectrum in water, *n*-hexane, and acetonitrile is accompanied by the appearance of the typical T_1 spectrum. For example, the 150 ps spectrum in *n*-hexane (part A in Figure 10) corresponds unambiguously to the T_1 spectrum observed at 30 ns (part A in Figure 3) although differences in the relative band intensities are noted, indicative of changes in the resonance enhancements, as expected from the different probe excitations used in the picosecond (380 nm) and nanosecond (355 nm) experiments. The low intensity of the 150 ps spectrum compared to the 10 ps one is consistent with the ratio of the T_1 and S_1 absorption strengths at 380 nm (see Figure 7). It results from the low T_1 yield in *n*-hexane as well as from the fact that the 380 nm probe wavelength is in much better resonance condition for the S_1 state than for T_1. On the other hand, the 150 ps Raman spectrum in methanol resembles remarkably the 40 ns spectrum displayed in Figure 5. It corresponds to the superposition of Raman bands due to the T_1 state and to the 4PPYH$^\bullet$ radical, in agreement with the above results from transient absorption. The time dependence of the different Raman components shows unambiguously that the 4PPYH$^\bullet$ radical is produced in parallel to the T_1 species from the S_1 state. The photoreactivity of 4PPY in alcohols is thus similar to that recently reported for its diaza analogue, 4,4′-bipyridine.[26] In both cases an hydrogen adduct radical is formed partly from the T_1 state via a mechanism of H atom abstraction from the alcoholic solvent, with rate constants of the order of 10^5 M^{-1} s^{-1}, and partly from the S_1 state with rate constants about 5 orders of magnitude higher. In the case of 4,4′-bipyridine, a first analysis, by subpicosecond transient absorption, of this surprisingly fast process in a series of alcoholic solvents and in binary solutions suggested a mechanism of H atom abstraction by the S_1 state arising within H-bonded solute/solvent entities via homolytic breaking of the H-bonded alcohol OH bond. However, in this assumption the formation of the *N*-hydro radical in *n*-hexane and the lack of radical formation in water remained unexplained. More recently, picosecond time-resolved Raman investigation[34] of the radical formed in the isotopically substituted solvents CH_3OD and CD_3OH indicated that H atom transfer in the S_1 state results, as in the T_1 state, from hydrogen abstraction from the methyl group of the donating alcohol molecule. The much lower rate constant observed for the reaction involving the T_1 state can be explained by the different natures of the S_1 and T_1 states (see below) and by the presence in the T_1 state of hydrogen bonding with the solvent, not expected in the S_1 state.[34]

Table 1 gives, for characteristic solvents, the S_1-state absorption maxima (λ_{max}) and the S_1 lifetime (τ_{S_1}) determined from the exponential fit of the absorption decay at 570 nm. To evaluate the solvent effect on the rate of intersystem crossing, $k_{ISC}(S_1 \rightarrow T_1)$, we give also in Table 1 relative values for the T_1 quantum yield ($\Phi_{T_1}^{rel}$). These values are calculated as the ratios of the T_1 band intensity at the end of the kinetics (500 ps spectrum) and of the initial S_1 band intensity estimated by extrapolating the exponential decay fit of the S_1 absorption to time zero, normalized relative to the value found for acetonitrile which is arbitrarily taken as unity. This procedure assumes that the T_1 and S_1 absorption strengths are independent of the solvent. Relative values for the ISC rate constants (k_{ISC}^{rel}) in the different solvents can thus be obtained by weighting the relative T_1 quantum yield values by the corresponding S_1 lifetimes according to the relation $\Phi_{T_1} = \tau_{S_1} k_{ISC}$. These values, normalized relative to that found in *n*-hexane, are given in Table 1. Similarly, the relative values given in Table 1 for the radical

TABLE 1: Absorption Peak Wavelengths of the Excited S_1 and T_1 States and of the *N*-Hydro Radical RH•, S_1 Lifetime, and Relative Values for the T_1 Quantum Yield, Intersystem Crossing Rate Constant, and RH• Quantum Yield of 4PPY in Various Solvents

solvent	$\lambda^{max}_{S_1 \rightarrow S_n}$ (nm)	$\lambda^{max}_{T_1 \rightarrow T_n}$ (nm)	$\lambda^{max}_{RH\bullet}$ (nm)	τ_{S_1} [a] (ps)	$\Phi_{T_1}^{rel}$ [b]	k_{ISC}^{rel} [c]	$\Phi_{RH\bullet}^{rel}$ [d]
CH_3CN	370, 575	352		100	1.0	0.81	
C_6H_{14}	368, 555	352	345, 515	22	0.27	1.0	0.2
H_2O	370, 575	357		84	0.9	0.87	
CH_3OH	370, 575	355	355, 530	28	0.3	0.87	1.0
2PrOH	370, 575	355	355, 530	30	0.4	0.93	0.6

[a] Value established from monoexponential decay fit of the of the S_1 absorption (accuracy ±5%). [b] $I^{T_1}_{370nm}(t=500\ ps)/I^{S_1}_{575nm}(t=0)$ ratio normalized wih respect to the value in acetonitrile. [c] Φ_{T_1}/τ_{S_1} ratio normalized with respect to the value in *n*-hexane. [d] $I^{RH\bullet}_{530nm}(t=500\ ps)/I^{S_1}_{575nm}(t=0)$ ratio normalized with respect to the value in methanol.

TABLE 2: Observed Resonance Raman Frequencies (cm^{-1}) and Assignments of the Ground State (S_0), First Triplet State (T_1), *N*-Hydro Radical (RH•), and First Excited Singlet State (S_1) of 4PPY; Corresponding S_0 and T_1 Raman Frequencies of Biphenyl (BP) and 4,4′-Bipyridine (44BPY) and the Raman Frequencies of the 4,4′-Bipyridine *N*-Hydro Radical (44BPYH•) Are Also Given for Comparison

	ground state S_0			triplet state T_1			*N*-hydro radical RH·		singlet state S_1
mode	4PPY	BP[a]	44BPY[b]	4PPY[c]	BP[d]	44BPY[e]	4PPYH·[f]	44BPYH·[g]	4PPY[h]
8a	1612	1612	1607	1562	1570	1544	1636[i]	1650[i]	1570
	1587	*1597*	*1589*				1574[j]	1587[j]	
19a	1513	1507	1511	1465	1476	1471	1495	1506	1482
	1480	*1482*	*1487*						
13	1283	1285	1297	1366	1366	1377	1309[i]	1337	1291
9a	1235	1190	1219		1205	1207	1212	1228[j]	1181
	1188	*1176*	*1218*				1178[i]	1198[i]	1139
18a	1044	1030	1088	940	964	1014	1033[i]	1055[i]	1025
	(1020)	*1040*	*1099*	1027					
12	1003	1003	1000	984	985		984[j]	997[j]	963
	(1020)	*1008*	*1038*	1027			1015	1019	
1	748	742	756				724	740[j]	710
	987	*965*	*989*				963[i]	967	
6a	332	315	315		334				
	610	*609*	*607*					590	

[a] From ref 11 (values in italics correspond to the nonsymmetric out-of-phase components). [b] From ref 27 (values in italics correspond to the nonsymmetric out-of-phase components). [c] Solvent *n*-hexane. [d] From ref 18 (solvent *n*-hexane). [e] From ref 25 (solvent acetonitrile). [f] Solvent methanol. [g] From ref 22 (solvent methanol). [h] Solvent *n*-hexane. [i] Band specifically enhanced on excitation at 532 nm in resonance with the visible absorption. [j] Band specifically enhanced on excitation at 370 nm in resonance with the UV absorption.

quantum yield ($\Phi_{RH\bullet}^{rel}$) are calculated as the ratios of the radical visible absorption intensity at 500 ps and of the initial S_1 band intensity, normalized relative to the value in methanol. Assuming a nondiffusional H-abstraction process, a first-order rate constant of $k_r \sim 2 \times 10^{10}\ s^{-1}$ is estimated from the change in S_1 lifetime on going from water to the alcohol solvent, according to the relation $k_r = [\tau_{S_1}(\text{alcohol}) - \tau_{S_1}(\text{water})]^{-1}$.

3.3. Vibrational Analysis of the S_1 and T_1 States of 4PPY and of the 4PPYH• Radical. Table 2 gives the frequencies and assignments of the resonance Raman bands observed for the T_1-state, S_1-state, and *N*-hydro radical of 4PPY and the corresponding ground-state vibrational features. The resonance Raman bands reported for the T_1 state of the neighboring molecules biphenyl[18] and 4,4′-bipyridine (44BPY),[25] and for the *N*-hydro radical 44BPYH•,[22] and the related S_0 components are also given in Table 2 for comparison. The notation adopted for designating the vibrations is that proposed by Varsanyi for monosubstituted benzenes,[35] already employed for pyridine,[36,37] biphenyl,[17,18] and 44BPY.[22,25] Since the Raman spectra of the transient states S_1, T_1, and 4PPYH• are probed in resonance with strongly allowed electronic absorptions, the scattering process can be considered as Franck−Condon controlled. Accordingly, only the totally symmetric modes along whose coordinates the resonant excited-state potential is displaced are expected to show a notable resonance Raman activity.

As biphenyl[38] and 44BPY,[27] S_0 4PPY is probably twisted in solution (symmetry C_2) due to steric hindrance by hydrogen atoms in position ortho to the inter-ring bond. The IR and Raman spectra of S_0 4PPY resemble closely those of biphenyl[39,40] and 44BPY,[27,41] and their complete assignment has been straightforwardly made by analogy. We do not present this assignment here. The S_0 vibrations given in Table 2 correspond to the 15 fundamental modes, excepting the CH stretches, which remain totally symmetric in the coplanar C_{2v} symmetry found (see below) for the transient species T_1, S_1, and RH•. These are the inter-ring stretch (mode 13) and, for each ring (phenyl and pyridyl), seven in-plane vibrations that are symmetric relative to the C_2 axis (8a, 19a, 9a, 18a, 12, 1, and 6a). In the centrosymmetric molecules, biphenyl and 44BPY, coupling between the two rings yields, for each ring mode, one totally symmetric (in-phase) component and one nonsymmetric (out-of-phase) component (indicated in italics in Table 2). In 4PPY, the benzene and pyridyl vibrational components having comparable energies, couplings also take place, and the two components of each ring mode can be considered as analogous to the above in-phase and out-of-phase components. Nevertheless, both are totally symmetric. This analogy is confirmed by the following observation: in biphenyl and 44BPY, the in-phase (totally symmetric) components of the ring distortion modes 1 and 6a are shifted down by about 230 and 300 cm^{-1}, respectively, relative to the value in benzene or pyridine, due to a strong coupling with the totally symmetric inter-ring stretching mode 13, whereas the out-of-phase component is unaffected (see Table 2, S_0 frequencies). A rigorously similar behavior is observed for the components of modes 1 and 6a in 4PPY.

The triplet-state Raman spectrum of 4PPY (spectrum A in Figure 3) is comparable concerning its resonance activity to

the spectra found for biphenyl[16−19] and 4,4′-bipyridine[24,25] in resonance with their respective $T_1 \rightarrow T_n$ absorption bands (370 and 340 nm, respectively). It shows six peaks in the 300−1800 cm^{-1} region. Five of them can be associated straightforwardly to five of the eight totally symmetric modes of the D_{2h} structure of T_1 biphenyl and T_1 44BPY and are assigned by analogy to the "in-phase" component of modes 8a, 19a, 18a, and 12 and to mode 13. Only one peak at 1027 cm^{-1} cannot correspond to an "in-phase" component and is ascribed to one of the "out-of-phase" components expected in this region (18a, 12, or 1). Its definitive attribution is not possible without the help of additional data from isotopomers. The dominant activity of the "in-phase" components denotes a near-D_{2h} symmetry for T_1 4PPY which indicates that the two rings are coplanar and structurally and electronically similar. The most intense lines are, as in the case of biphenyl and 44BPY, due to modes 8a, 19a, 13, and 18a. Modes 9a and 6a, extremely weak in the spectra of biphenyl and 44BPY, are not detected for 4PPY. Mode 1 remains unobserved for the three molecules. This analogous resonance Raman activity indicates that similar structural distortions take place in the three molecules on going from the T_1 state to the resonant T_n and thus that the $T_1 \rightarrow T_n$ transition around 350 nm has the same origin in all cases. The T_1 frequencies of 4PPY, biphenyl, and 44BPY are comparable (see Table 2). The main variations on going from S_0 to T_1 are the decrease in frequency of most of the ring modes and the increase by 83 cm^{-1} of the frequency of mode 13 (81 and 80 cm^{-1} for biphenyl and 44BPY, respectively) which contains a large contribution of the inter-ring stretching coordinate. These shifts characterize a decrease of the π-bonding on the rings and a strengthening of the inter-ring bond, i.e., the appearance of a quinoidal distortion, comparable in the three molecules, which confirms the coplanar conformation of the T_1 state.

The Raman spectra of the *N*-hydro radical 4PPYH$^{\bullet}$ (part B in Figure 3) are comparable to those previously obtained for the *N*-hydro radical of 4,4′-bipyridine (44BPYH$^{\bullet}$) in regard to the activity, the peak frequencies, and the relative resonance intensity enhancements. As seen in Table 2, except for mode 6a which is very weak in 44BPYH$^{\bullet}$ and is not detected in 4PPYH$^{\bullet}$, the Raman activity is strictly similar in the two radicals. The observation in both cases, in contrast to the T_1 species, of two components for modes 8a, 9a, 12, and 1, one being resonance enhanced upon UV probing and the second upon visible probing, is indicative of two significantly dissimilar rings. In particular, a much larger splitting is noted for mode 8a in the *N*-hydro radical (62 cm^{-1} in 4PPYH$^{\bullet}$, 63 cm^{-1} in 44BPYH$^{\bullet}$) than in the parent S_0 species. According to the previous discussion reported for 44BPYH$^{\bullet}$,[22] the lower and higher energy components can be considered as mostly localized in the nonprotonated and protonated rings, respectively, the high frequency of the protonated pyridyl component being typical of a pyridinium configuration. This differentiation of the two rings is analogous in 4PPYH$^{\bullet}$ and 44BPYH$^{\bullet}$, which accounts for the similarity of the resonance Raman spectra. The frequency differences observed for the remaining vibrations (19a, 13, 18a) between the S_0 molecule and the *N*-hydro radical are weak and cannot be interpreted, even qualitatively, in terms of structural distortions without the help of further analyses by quantum calculations. We suggest nevertheless that the positive frequency shift of mode 13 (+26 and +40 cm^{-1} for 4PPYH$^{\bullet}$ and 44BPYH$^{\bullet}$) relative to the parent molecule, though much smaller than that found in the T_1 state, reflects some reinforcement of the inter-ring bond. This conclusion and the lack of out-of-plane mode active in the resonance Raman spectra, whichever the probe excitation, are indicative of a planar structure of C_{2v} symmetry for 4PPYH$^{\bullet}$ as for 44BPYH$^{\bullet}$.

Finally, the S_1-state Raman spectrum of 4PPY (10 ps spectra in Figure 10) shows eight bands in the 300−1800 cm^{-1} region. They can be straightforwardly ascribed to the ring modes 8a, 19a, 9a, 18a, 12, and 1, and to mode 13, by analogy with the ground-state spectrum. Only mode 9a presents distinctly two components at 1181 and 1139 cm^{-1} which correspond to the "in-phase" and "out-of-phase" components. As in the T_1 state, the ring vibrations are notably shifted to lower frequencies with respect to the S_0 state, as expected from the presence of an electron in a π^* orbital. These shifts are not very different from those of the T_1 state. However, an essential difference between the T_1 and S_1 spectra concerns the frequency of mode 13. Whereas this mode was shown above to be the most sensitive to the $S_0 \rightarrow T_1$ transition with a 83 cm^{-1} shift to higher frequency, it appears almost insensitive in the $S_0 \rightarrow S_1$ transition. The inter-ring bond remains thus essentially a single bond in the S_1 state. Therefore, no delocalization is to be expected between the two rings and, although no out-of-plane vibration is detected, a nonplanar conformation of S_1 4PPY with a significant inter-ring twist angle is not improbable. These observations suggest that the electronic nπ^* excitation might be localized in the pyridyl ring whereas it is delocalized on the two rings through the quinoidal distortion in the T_1 state. In this respect, the radical structure for which the inter-ring bond is only weakly strengthened relative to the ground state is closer to the S_1 structure than to the T_1 one. A more detailed analysis of the S_1 and T_1 vibrational properties, including time-resolved Raman measurements at different probe wavelengths and sophisticated quantum calculations, is in progress to confirm this point.

3.4. Nature of the Excited S_1 and T_1 States. A $\pi\pi^*$ configuration derived from that of biphenyl has been proposed for the T_1 state of 44BPY from electron paramagnetic resonance[42] and transient Raman[24] data. The above-mentioned resemblance of the T_1-state Raman spectra of 4PPY, biphenyl, and 44BPY (resonance activity and frequency variations relative to S_0) indicates undoubtedly that T_1 4PPY has also a $\pi\pi^*$ configuration derived from that of triplet biphenyl, characterized by a near-D_{2h} coplanar conformation of the rings and a quinoidal distortion with significant increase of the inter-ring bond order. As a confirmation, the $T_1 \rightarrow T_n$ absorption of 4PPY presents a notable analogy with that of biphenyl (λ_{max} = 370 nm, $\tau_{1/2}$ = 130 μs in hexane at 300 K[12,13]) and of 44BPY (λ_{max} = 340 nm, $\tau_{1/2}$ = 70 μs in acetonitrile at 300 K[21,23]). This conclusion of a $\pi\pi^*$ nature for the T_1 state of 4PPY is in accord with previous analyses from phosphorescence[3,4] and EPR[6] measurements and with CNDO predictions.[4]

Several experimental features, which we discuss below, lead us to consider that the S_1 state of 4PPY is essentially of nπ^* character in all the solvents investigated in this work apart in TFE and in H_2O/HCl solutions. A first essential point is the resemblance of the S_1 absorption spectra in alkanes, alcohols, water, and acetonitrile: after the spectral relaxation observed in a 0−20 ps time range, which will be discussed later, the S_1 spectra in protic solvents such as methanol (10 ps spectrum in Figure 9) and water (20 ps spectrum in Figure 8) are nearly identical (bands relative intensity and position) to that in acetonitrile. A comparable spectrum is also observed in nonpolar alkanes (3 ps spectrum in Figure 7), despite a 20 nm blue shift of the visible band ascribable to solvent polarity effects. Such a shift has been observed for the S_1 state of 4,4′-bipyridine on going from polar to nonpolar solvents.[26] Similarly, the same S_1-state resonance Raman spectrum is found in

water, methanol, ethanol, acetonitrile, and *n*-hexane. This ensemble of spectroscopic observations shows undoubtedly that the geometry and electronic structure, and thus the nature, of the S_1 state of 4PPY are similar in these solvents. In particular, hydrogen bonding of the ground-state molecule in alcohols and water does not affect the nature of the S_1 state.

There is a manifest resemblance between the S_1 absorption spectrum of 4PPY and those found for 44BPY (λ_{max} = 374, 580 nm in acetonitrile) and 22BPY (λ_{max} = 363, 530 nm in acetonitrile) which have been ascribed to nπ^* states.[26] On the other hand, the $S_1(\pi\pi^*)$ spectrum of biphenyl, characterized by a strong visible band at 655 nm[15,43] and a weaker one at 395 nm,[43] is notably different. These observations suggest a S_1-state nπ^* character for 4PPY as for 44BPY and 22BPY. Another indication in favor of this conclusion is the resemblance of the S_1 absorption and resonance Raman spectra with the corresponding spectra of the *N*-hydro radical 4PPYH$^\bullet$. In fact, from simple molecular orbital considerations, the electronic configuration of the nπ^* S_1 state is expected to be analogous, concerning the π electron distribution, to that of the *N*-hydro radical or of the anion radical (all π orbitals occupied and one π^* electron in the lowest unoccupied orbital).

Consider now the dependence of the S_1 lifetime and T_1 quantum yield on the solvent nature (Table 1). As was observed for 44BPY and 22BPY,[26] the S_1 lifetime of 4PPY ($\tau_{S_1} \leqslant 100$ ps) is much shorter than the S_1 state of biphenyl (16 ns in *n*-hexane at 300 K[19]) in all solvents. This shortness is consistent with the low yield of fluorescence of the aza-aromatic derivatives. Although the S_1 lifetime varies from 20 to 100 ps depending on the solvent, the relative value, k_{ISC}^{rel}, calculated for the rate constant of intersystem crossing is not significantly solvent dependent. ISC is thus not the process responsible for the fluctuations of the S_1 lifetime in the different solvents. Absolute T_1 yields are not known, but assuming a maximum value (in acetonitrile) of the same order than those reported for 2,2′-bipyridine (Φ_{T_1}= 0.83[29]) or biphenyl (Φ_{T_1}= 0.84[14]) allows an estimate of the ISC rate constant, $k_{ISC} = \Phi_{T_1}/\tau_{S_1}$, of about 0.8×10^{10} s^{-1}. Such a high $S_1 \rightarrow T_1(\pi\pi^*)$ rate is consistent with a nπ^* configuration of the S_1 state in regard to El-Sayed's prediction that fast ISC must occur between nπ^* and $\pi\pi^*$ states of *N*-heterocyclics due to allowed spin−orbit coupling[8] and favorable Franck−Condon overlaps.[7]

In summary, the absence of significant gain signal, the fast ISC rate constant, the nearly independent magnitude of this constant upon the solvent nature, and the similarity of the S_1 absorption and resonance Raman spectra in all solvents confirm unambiguously that the nπ^* nature of the S_1 state of 4PPY remains unchanged on going from alkanes to alcohols, acetonitrile, and water. In contrast, the appearance of a strong gain spectrum in the acidic TFE and water/HCl solutions suggests that, due to strong hydrogen bonding or even excited-state protonation of 4PPY, the nπ^* character of the S_1 state is lowered to the benefit of a $\pi\pi^*$ configuration for which ISC to the $T_1(\pi\pi^*)$ state is expected to be much slower. These results are thus in disagreement with the report by Hotchandani and Testa[4] stating that 4PPY fluoresces in water with the same yield (Φ_F = 0.19) as in acidic media (Φ_F = 0.20). The authors conclude that excited-state protonation of 4PPY takes place in water as in acidic media, resulting in an inversion of close-lying nπ^* and $\pi\pi^*$ states. In this hypothesis the S_1 state should be equivalent to the $S_1(\pi\pi^*)$ state of biphenyl (Φ_F = 0.18[20]), and a S_1 lifetime of a few nanoseconds should characterize 4PPY in water, which is in manifest contradiction with our observations by transient absorption and resonance Raman. The reason of this discrepancy concerning the photophysical reactivity of 4PPY in water is not clear. As regards to the strong intensity of the transient absorption spectra ascribed above to the S_1 state and according to the high reproducibility of the measurements which have been checked repeatedly, the characterization of the S_1 state and its related lifetime analyses cannot be contested. The discrepancy mentioned above could eventually result from differences in sample concentration between the two experiments since it is known that aromatic hydrocarbons may form aggregates in solution depending on their concentration. However, this point cannot be checked as no indication of sample concentration is given in the report of Hotchandani and Testa.

3.5. Short Time Dynamics in Water and Alcohols. As mentioned above, the decay of the S_1-state absorption is preceded at short time by a solvent-dependent spectral evolution. In acetonitrile (Figure 6), a small absorption increase of the S_1 band maxima takes place between 1 and 15−20 ps. In combination with this rise in intensity, a slight band narrowing is perceptible on the red band edge which results in an intensity decrease in the band wing regions 400−430 and 620−650 nm. These effects are typical of vibrational relaxation processes. As a matter of fact, since an upper state $S_n(\pi\pi^*)$ is initially populated on excitation, hot $S_1(n\pi^*)$ species are likely produced by internal conversion and vibrational cooling is expected. In *n*-hexane (Figure 7), the S_1 lifetime being much shorter (22 ps), the 1−20 ps spectral evolution is dominated by the decay of the S_1 population.

In contrast, the short-time dynamics in water and alcohols is characterized by large spectral changes (Figures 8 and 9). The visible absorption undergoes a notable frequency shift from a region beyond 650 nm (1 ps delay) to the final position at 575 nm (delay $\geqslant$ 10 ps). This effect may be either a real shift of the S_1 band profile or the result of the decay of an initial precursor band in the IR region in parallel to the rise of the S_1 band. The short time dependence of the UV band profile is less pronounced but can also be perceived either as a substantial narrowing of the red band edge or as the decay of a second absorption component present as a shoulder in the 400−450 nm region. These effects indicate the existence of a short-time relaxation process specific to the protic solvents. Their interpretation must account for this solvent specificity and for the fact that the relaxed S_1 absorption spectrum is comparable to that directly obtained in aprotic solvents. It is unlikely that vibrational relaxation of a hot S_1 state is responsible for the observed spectral evolution at short delay times since it cannot explain the considerable difference of behavior between aprotic and protic solvents. A reduction of the vibrational relaxation effect is rather expected in protic solvents if we consider that the $^1n\pi^*$ state is less stabilized than in aprotic solvents. This conclusion is consistent with the fact that no anti-Stokes Raman intensity could be detected in the 2−20 ps time range. The solvent dependence suggests that hydrogen bonding plays a role in the relaxation process. A possible explanation is that of reorganization of the solvent cage in the S_1 state. In fact, whereas the ground-state S_0 and the initially excited-state $S_n(\pi\pi^*)$, zwitterionic in nature, are stabilized by the formation of a hydrogen bond between the lone pair orbital of 4PPY and the protic solvent, in the $S_1(n\pi^*)$ state the lone pair orbital is depleted of an electron, eliminating the possibility of hydrogen bonding. The short time dynamics observed in water and alcohols can thus be due to the relaxation of the [S_1 4PPY/solvent cage] conformation accompanying the break of the H bond.

An alternative explanation is that the observed short time spectral change in water and alcohols corresponds to the $S_n(\pi\pi^*) \rightarrow S_1(n\pi^*)$ electronic relaxation itself. In fact, since hydrogen

bonding stabilizes the S_n state but not the S_1 state, a slowdown of the kinetics of internal conversion can be expected in protic solvents, in agreement with the solvent specificity that is observed (i.e., internal conversion is assumed to be completed at 1 ps in alkanes and acetonitrile solutions). In this assumption the S_n state would be characterized by two absorption bands lying around 400 and 700 nm, with intensities respectively higher and lower than the related S_1 bands at 370 and 575 nm. A certain analogy between this S_n spectrum and the $S_1(\pi\pi^*)$ spectrum of biphenyl, which presents a strong band at 655 nm[15,43] and a weaker one at 395 nm,[43] is consistent with this interpretation. However, our observation that the Raman spectrum probed at 400 nm is similar to the S_1 spectrum obtained at 370 nm even at short delay time (2 ps) deserves the attribution of the 400−450 nm shoulder to a different excited state, unless a much weaker resonance Raman enhancement effect for this state than for the S_1 state is assumed at 400 nm.

Both the interpretations proposed above for the short time dynamics of 4PPY in protic solvents involve the relaxation from a state where the molecule is H-bonded to the solvent toward a state where the H bond is released. A rigorous interpretation of this effect needs more experimental work than presented here. In particular, a quantitative analysis of the kinetics at various wavelengths is indispensable. Further work is planned to extend the present study to the red spectral domain and to monitor the short time kinetic response of the transient absorption as a function of the wavelength in a series of solvents and in binary solutions.

4. Conclusion

The structural changes and relaxation dynamics of 4-phenylpyridine (4PPY) following UV pulsed photoexcitation have been probed in various solvents by using transient absorption and time-resolved resonance Raman spectroscopies in the nanosecond and picosecond time domains. The T_1 and S_1 states are characterized as $\pi\pi^*$ and $n\pi^*$ states, respectively, in aprotic solvents as well as in alcohols and water. In acidic solutions a fluorescent $\pi\pi^*$ S_1 state is evidenced. Conversely to 4,4′-bipyridine, 4PPY is not photoreduced via electron transfer by amines such as triethylamine. In contrast, photoreduction via H atom abstraction by the T_1 state ($k \sim 10^5$ M^{-1} s^{-1}) and the S_1 state ($k \sim 10^{10}$ M^{-1} s^{-1}) arises in alcohols as for 4,4′-bipyridine and yields the *N*-hydro radical, 4PPYH$^\bullet$. The considerably higher reactivity of the S_1 state compared to that of T_1 can be accounted for first by the $n\pi^*$ nature of S_1. On the other hand, considering the occupancy of the nitrogen n orbital, hydrogen bonding with the solvent is probable in the $\pi\pi^*$ T_1 state but cannot arise in the $n\pi^*$ S_1 state. The difference in reactivity of the S_1 and T_1 states can thus be also explained by a hindrance in the T_1 state of the H atom transfer process by H bonding. Finally, the qualitative analysis of the time-resolved Raman spectra of the 4PPYH$^\bullet$ radical, T_1, and S_1 species shows that the radical and S_1 structures are both characterized by weak electronic delocalization between the two molecular rings whereas the T_1 state presents in contrast a highly delocalized geometry with notable quinoidal distortion and double-bond character of the inter-ring bond. A much lower change in molecular geometry is thus expected in the $S_1 \rightarrow$ radical process than in the $T_1 \rightarrow$ radical reaction, which is a further argument in agreement with the higher reactivity of S_1 in the hydrogen atom abstraction process. A more quantitative interpretation of the vibrational data of these transient species in terms of structure and conformation is in progress by means of ab initio calculations.

Acknowledgment. The Centre d'études et de Recherches Lasers et Applications (CERLA) is supported by the Ministère chargé de la Recherche, Région Nord/Pas de Calais, and the Fonds Européen de Développement Economique des Régions.

References and Notes

(1) Becker, R. S. *Theory and Interpretation of Fluorescence and Phosphorescence*; Wiley: New York, 1969.

(2) Lim, E. C. *Excited States*; Academic: New York, 1977; Vol. 3, p 305.

(3) Yagi, M.; Matsunaga, M.; Higuchi, J. *Chem. Phys. Lett.* **1982**, *86*, 219.

(4) Hotchandani, S.; Testa, A. C. *J. Photochem. Photobiol.* **1991**, *A55*, 323.

(5) Kubin, J.; Testa, A. C. *J. Photochem. Photobiol.* **1994**, *A83*, 91.

(6) Yagi, M.; Itoh, I.; Komura, A.; Hayashi, K.; Higuchi, J. *Chem. Phys. Lett.* **1993**, *211*, 179.

(7) El-Sayed, M. A. *J. Chem. Phys.* **1962**, *36*, 573.

(8) El-Sayed, M. A. *J. Chem. Phys.* **1963**, *38*, 2834.

(9) Sarkar, A.; Chakravorti, S. *J. Lumin.* **1995**, *65*, 163.

(10) Li, R.; Lim, E. C. *J. Chem. Phys.* **1972**, *57*, 605.

(11) Zerbi, G.; Sandroni, S. *Spectrochim. Acta* **1968**, *24A*, 483.

(12) Land, E. J. *Proc. R. Soc. London, A* **1968**, *305*, 457.

(13) Heinzelmann, W.; Labhart, H. *Chem. Phys. Lett.* **1969**, *4*, 20.

(14) Amand, B.; Bensasson, R. *Chem. Phys. Lett.* **1975**, *34*, 44.

(15) Kato, C.; Hamaguchi, H.; Tasumi, M. *Chem. Phys. Lett.* **1985**, *120*, 183.

(16) Hamaguchi, H. In *Vibrational Spectra and Structure*; Durig, J. R., Ed.; Elsevier: Amsterdam, 1987; Vol. 16, p 272.

(17) Buntinx, G.; Benbouazza, A.; Poizat, O.; Guichard, V. *Chem. Phys. Lett.* **1988**, *153*, 279.

(18) Buntinx, G.; Poizat, O. *J. Chem. Phys.* **1989**, *91*, 2153.

(19) Sasaki, Y.; Hamaguchi, H. *Spectrochim. Acta* **1994**, *50A*, 1475.

(20) Murov, S. L.; Carmichael I.; Hug, G. L. *Handbook of Photochemistry*; Dekker: New York, 1993.

(21) Elisei, F.; Mazzucato, U.; Görner, H.; Schulte-Frohlinde, D. *J. Photochem. Photobiol.* **1989**, *50A*, 209.

(22) Poizat, O.; Buntinx, G.; Ventura, M.; Lautié, M. F. *J. Phys. Chem.* **1991**, *95*, 1245.

(23) Buntinx, G.; Valat, P.; Wintgens, V.; Poizat, O. *J. Phys. Chem.* **1991**, *95*, 9347.

(24) Poizat, O.; Ventura, M.; Buntinx, G. *Spectrosc. Lett.* **1990**, *23*, 701.

(25) Poizat, O.; Buntinx, G.; Valat, P.; Wintgens, V.; Bridoux, M. *J. Phys. Chem.* **1993**, *97*, 5905.

(26) Buntinx, G.; Naskrecki, R.; Poizat, O. *J. Phys. Chem.* **1996**, *100*, 19380.

(27) Ould-Moussa, L.; Poizat, O.; Castella-Ventura, M.; Buntinx, G.; Kassab, E. *J. Phys. Chem.* **1996**, *100*, 2072.

(28) Buntinx, G.; Poizat, O.; Valat, P.; Wintgens, V.; Righini, R.; Foggi, P. *J. Chim. Phys.* **1993**, *90*, 1733.

(29) Saini, R. D.; Dhanya, S.; Bhattacharyya, P. K. *J. Photochem. Photobiol.* **1988**, *43A*, 91.

(30) Poizat, O.; Locoge-Karbowski, N.; Buntinx, G. *Trends Phys. Chem.* **1991**, *2*, 199.

(31) Buntinx, G.; Poizat, O.; Leygue, N. *J. Phys. Chem.* **1995**, *99*, 2343.

(32) Allet, C.; Buntinx, G.; Locoge-Karbowski, N.; Poizat, O. *J. Phys. IV* **1991**, *1(SC7)*, 463.

(33) Tabner, B. J.; Yandle, J. R. *J. Chem. Soc. A* **1968**, 381.

(34) Didierjean, C.; Buntinx, G.; Poizat, O. Submitted for publication.

(35) Varsanyi, G. *Assignments for Vibrational Spectra of Benzene Derivatives*; Land, I., Ed.; Adam Hilger: London, 1974; Vol. 1.

(36) Wilmshurst, J. K.; Bernstein, H. J. *Can. J. Chem.* **1957**, *35*, 1183.

(37) Ajito, K.; Takahashi, M.; Ito, M. *Chem. Phys. Lett.* **1989**, *158*, 193.

(38) Eaton, V. J.; Steele, D. *J. Chem. Soc., Faraday Trans. 2* **1973**, 1601.

(39) Zerbi, G.; Sandroni, S. *Spectrochim. Acta* **1968**, *24A*, 483; **1970**, *26A*, 1951.

(40) Bree, A.; Pang, C. Y.; Rabeneck, L. *Spectrochim. Acta* **1971**, *27A*, 1293.

(41) Topaçli, A.; Akyüz, S. *Spectrochim. Acta* **1995**, *51A*, 633.

(42) Gondo, Y.; Maki, A. H. *J. Phys. Chem.* **1968**, *72*, 3215.

(43) Didierjean, C.; Bussotti, L.; Buntinx, G.; Poizat, O. Unpublished results.